UNDOPED AND LIGHTLY DOPED SQUARE-LATTICE QUANTUM ANTIFERROMAGNET

Efstratios Manousakis

Department of Physics and Center for Materials Research and Technology
Florida State University, Tallahassee, Florida 32306

ABSTRACT

We review numerical and analytical results obtained on the strong-coupling Hubbard Hamiltonian and the related spin-1/2 antiferromagnetic (AF) Heisenberg and quantum nonlinear σ models (QNLσM) on a square lattice. Our studies of the AF Heisenberg model and the equivalent QNLσM suggest that the ground state of the former is characterized by AF long-range order with sublattice magnetization and excitation spectrum consistent with spin-wave theory and experiments. At low temperatures the correlation length calculated from the AF Heisenberg model behaves as $\xi(T) = ae^{b/T}$; the same behavior is also found in the ordered phase of the QNLσM. Using a value $J = 1270K$ for the AF coupling, this form fits the temperature-dependent correlation length obtained from neutron scattering experiments done on La_2CuO_4. Furthermore, we study the role of mobile holes introduced by doping the strong-coupling Hubbard Hamiltonian. We discuss the excitation spectrum of a single hole obtained by exact diagonalizations and by variational calculations. We find a parameter range where hole-pairing is energetically favorable in the model.

1. Introduction

The suggestion that the superconductivity mechanism in the copper-oxide materials may be understood by studying the two-dimensional Hubbard-model in its strong Coulomb repulsion limit[1] has recently received significant attention. Low-order strong-coupling perturbation treatment of the Hubbard model produces an

effective Hamiltonian[2] which operates in a restricted Hilbert space having states with no double-occupancy below half-filling

$$H_{eff} = H_1 + H_2 + H_3, \tag{1.1}$$

$$H_1 = -t \sum_{<i,j>,\sigma} (c^{\dagger}_{i,\sigma} c_{j,\sigma} + h.c), \tag{1.2}$$

$$H_2 = -2\frac{t^2}{U} \sum_{<i,j>,\sigma} \left(c^{\dagger}_{j,\sigma} c_{i,\sigma} n_{i,-\sigma} c^{\dagger}_{i,\sigma} c_{j,\sigma} + c^{\dagger}_{j,-\sigma} c_{i,-\sigma} c^{\dagger}_{i,\sigma} c_{j,\sigma} \right), \tag{1.3}$$

$$H_3 = -\frac{t^2}{U} \sum_{<i,j,k>,\sigma} \Big(c^{\dagger}_{k,\sigma} c_{j,\sigma} n_{j,-\sigma} c^{\dagger}_{j,\sigma} c_{i,\sigma} + c^{\dagger}_{k,-\sigma} c_{j,-\sigma} c^{\dagger}_{j,\sigma} c_{i,\sigma} + (i \rightarrow k, k \rightarrow i) \Big), \tag{1.4}$$

where $n_{i,\sigma} = c^{\dagger}_{i\sigma} c_{i\sigma}$, t is the hopping matrix element and U the on-site Coulomb repulsion. The first term (H_1) produces the constrained hole-hopping which avoids double occupancy. The second term (H_2) is obtained from the Hubbard model by integrating out virtual processes in which the electron hops, momentarily, to a neighboring site occupied by an electron of opposite spin and in the final state the two electrons go either in the original configuration or in the one with spins exchanged. Exact diagonalizations of small size systems[3] show that the three-site term (H_3) gives negligible contributions to the single-hole and two-hole energies. Ignoring the three-site interaction term and substituting U by $4t^2/J$ in the H_2 term, this effective Hamiltonian is now known as the $t-J$ model. The $t-J$ Hamiltonian is an interesting model on its own and its derivation from the Hubbard model may serve as a motivation[4].

At half-filling the H_1 and H_3 terms of the Hamiltonian (1.1) are inactive and H_2 (apart from a constant) reduces to the spin-1/2 antiferromagnetic (AF) Heisenberg model on the square-lattice

$$H = J \sum_{<i,j>} \left(S^z_i S^z_j + \frac{1}{2}(S^+_i S^-_j + S^-_i S^+_j) \right). \tag{1.5}$$

where $S^z_i = \frac{1}{2}(c^{\dagger}_{i\uparrow} c_{i\uparrow} - c^{\dagger}_{i\downarrow} c_{i\downarrow})$, $S^+_i = c^{\dagger}_{i\uparrow} c_{i\downarrow}$ and $S^-_i = c^{\dagger}_{i\downarrow} c_{i\uparrow}$. In the derivation from the single-band Hubbard model, $J = 4t^2/U$. However, the Hamiltonian (1.5) can be obtained form multi-band models also; hence the magnitude of the characteristic energy scale J of the model may be determined from the magnetic properties of the undoped materials. In two space dimensions (2D) the Heisenberg model cannot develop long-range-order (LRO) at any non-zero temperature[5]. Furthermore, there are no exact statements yet[6] about the existence of LRO in the ground state of the $s = 1/2$ antiferromagnet on the square lattice. Spin-wave theory (SWT), assumes the existence of AF LRO in the ground state and treats the zero-point motion of small

quantum fluctuations about the classical Nèel state perturbatively[7]. This picture is supported by several systematic approaches including analytical[7,8], semianalytical[9] and purely numerical techniques[10,11,12].

In the first part of this paper, we obtain a variational ground-state wave-function consistent with sum-rules for the dynamic structure function which gives accurate ground state properties. Using this wave-function and sum-rules we determine the spin-wave velocity[8,13]. The spin-wave velocity, the sublattice magnetization and the AF coupling J are accessible to experiments[14,15] and this allows direct test of the theory.

To make contact with the phenomenological properties of the copper-oxides, we need calculations on these models at non-zero temperature also. For instance, neutron scattering experiments performed on the undoped La_2CuO_4 [14] reveal strong two-dimensional spin correlations. The idea that the Hamiltonian (1.1) may be relevant for the physics behind these materials is supported by the comparison of the correlation length $\xi(T)$ obtained from a quantum Monte Carlo (QMC) study of the Hamiltonian (1.5) at finite temperature[16] with that inferred by neutron scattering experiments. At low temperatures, where $\xi(T)$ is much larger than the lattice spacing, the model (1.5) in two-space dimensions has the same long-wavelength limit with the quantum nonlinear σ model (QNLσM) [17]. Chakravarty, Halperin, and Nelson (CHN) studied the QNLσM by Renormalization Group with the β-function calculated with weak-coupling perturbation theory up to one[18] and two[19] loops. Their one-loop calculation suggests the form $\xi(T) = a/Te^{b/T}$ at low temperatures[18] and varying the parameters a and b CHN fit the neutron scattering data. This form, however, does not fit the $\xi(T)$ obtained from the QMC calculation of the Heisenberg model[16]. Later, the two-loop calculation[19] of CHN gives a different prefactor namely, $\xi(T) = ae^{b/T}$. To find the correct behavior of $\xi(T)$ and to make contact between the two models, we simulated the QNLσM on large lattices[20]. We found that in the ordered phase of the QNLσM, $\xi(T)$ can be approximated by the second form which also agrees with $\xi(T)$ obtained from the QMC study of the Heisenberg model. Furthermore, our $\xi(T)$ agrees reasonably well with the neutron scattering data using $J = 1270K$. We conclude that SWT correctly describes the $T = 0$ properties of the Heisenberg model and the 2D thermal spin correlations in the model are consistent with those observed by neutron scattering. Therefore the Hamiltonian (1.5) may be a part of the microscopic Hamiltonian necessary to understand the magnetic properties of the materials.

Due to the fact that the simulation of the model (1.1) is hindered by problems arising from the fermion statistics, the information about the phase diagram and superconductivity in the model is limited. Numerical studies of the model[26] suggest that a small amount of holes destroys the AF LRO. Recently this model has been studied by means of analytical and semianalytical approaches[21,22,23] as well as exact numerical diagonalization techniques[3,24,25]. These studies indicate that the creation of a hole inside the square-lattice spin-1/2 Heisenberg antiferromagnet leads to a well-defined quasiparticle excitation separated by a gap from an incoherent spectrum of spin-excitations. In this paper, we also report certain results for the

single-hole band obtained by VMC methods[27]. Exact diagonalization studies[3] on small-size system indicate that there is a range of t/U where hole-pairing is possible. These results have been reproduced later[25] and extended on a somewhat larger-size lattice.

In the next section we review results for the ground state and elementary excitations of the Hamiltonian (1.5) obtained by paired-magnon analysis and VMC calculations. In section 3 we discuss the properties of this model at low temperatures and its connection to the QNLσM. In the last section we discuss results on the full Hamiltonian (1.1) at very light doping obtained by VMC and exact diagonalization techniques.

2. Ground State and Elementary Excitations at Half-Filling

In the early fifties Anderson followed by Kubo, extended the spin-wave theory (SWT) introduced by Holstein and Primakoff for ferromagnets, to study the ground state of antiferromagnets with large spin s[7]. This technique, assumes the existence of AF LRO in the ground state and treats the zero-point motion of small quantum fluctuations about the classical Nèel state perturbatively. Initially this approach was thought to be an expansion in powers of $1/s$. Since the role of quantum fluctuations becomes more important for small s, it is natural to raise doubts about the convergence of this approach for the smallest possible spin case — the $s = 1/2$ antiferromagnet which is the case of our interest. Looking at the problem from a somewhat different angle it has been realized that the result of SWT is the leading order in a perturbation theory expansion in the number of loops which is also an expansion in powers of $1/z$, z being the coordination number. Still, this expansion is valid for higher dimensional lattices where z is large and the fluctuations are suppressed.

Recently there is significant effort to understand the square-lattice quantum Heisenberg antiferromagnet. Even though there are attempts to show the existence or non-existence of AF LRO in its ground state[6], the situation is not rigorously clear yet. Huse, by making a more accurate extrapolation to the $J^{\perp}/J^{z} = 1$ limit of the results of cumulant expansions[9] in powers of $J^{\perp}/J^{z}$, finds $m^{\dagger} \simeq 0.313$ for the staggered magnetization and $\frac{E_0}{dNJ} = -0.334 \pm 0.001$ for the ground state energy per bond. These results compare very well with those obtained from SWT[7] which are respectively, 0.303 and -0.332. Monte Carlo (MC) calculations also suggest that the picture obtained from SWT is correct. From the scaling behavior of the staggered magnetization, Reger and Young (RY) [11], using the Path Integral Monte Carlo (PIMC) technique on up to 12×12 size-systems, concluded that $m^{\dagger} \simeq 0.30 \pm 0.01$ in good agreement with SWT. Using the Green's function Monte Carlo (GFMC) method, Carlson and independently Trivedi and Ceperley have performed accurate simulations[12] on up to 32×32 lattice size. They find that the ground-state energy per bond and staggered magnetization follows the finite-size scaling expected from SWT. Their extrapolated values to the infinite lattice are $\frac{E_0}{dNJ} = -0.3349 \pm 0.0001$

and $m^{\dagger} \simeq 0.31 \pm 0.01$. Furthermore, they studied spin-wave states and concluded that the energy-gap scales as predicted by SWT and vanishes in the infinite-lattice limit.

In this section we shall review certain results obtained with the variational approach. In Ref.8, we used a complete set of multi-magnon states and calculated the matrix elements of the Hamiltonian (1.5) in a separability approximation originally developed for the treatment of strongly correlated quantum liquids [28]. The multi-magnon states may be defined as

$$|...n(k)...) \equiv \prod_{\vec{k}} (\sigma^z_{\vec{k}})^{n(k)} |\phi>, \tag{2.1.a}$$

$$\sigma^z_{\vec{k}} = \frac{1}{\sqrt{N}} \sum_{\vec{R}} e^{i\vec{k}.\vec{R}} \sigma^z_{\vec{R}}, \tag{2.1b}$$

where the sum is over all N lattice vectors $\vec{R}$ and $n(k) = 0, 1, 2, ..., N$. The state $|\phi>$ is defined as follows:

$$|\phi> \equiv \frac{1}{\sqrt{2^N}} \sum_c (-1)^{L(c)} |c> . \tag{2.2}$$

Here the sum is over all possible spin configurations c and $L(c)$ is the number of down spins in one sublattice contained in the configuration c. The state $|\phi>$ can be written as $|\phi> = \prod_{\vec{R}\epsilon A} |\vec{R}, +> \prod_{\vec{R}\epsilon B} |\vec{R}, ->$ and the states $|\vec{R}, +>$ and $|\vec{R}, ->$ are the eigenstate of $\hat{S}^x_{\vec{R}}$. A and B represent the two sublattices. It can be easily verified that the state (2.2) has zero staggered magnetization in the z and y directions but has full staggered magnetization in the x direction. In fact, if we rotate the Nèel state around the y-axis by $\pi/2$ we obtain the state (2.2).

These states form a complete but non-orthogonal set. Let us first consider the subspace of m magnons occupying the state with momentum $\vec{k}$ and n magnons occupying the state having momentum $-\vec{k}$. We modify the definition as follows

$$|m, n> \equiv \sqrt{\frac{[N-(m+n)]!}{m!n!N!}} \sum_{\{\vec{R}_i, \vec{r}_j\}_C} e^{i\vec{k}.(\vec{R}_1+...+\vec{R}_m)} e^{-i\vec{k}.(\vec{r}_1+...+\vec{r}_n)} \sigma^z_{\vec{R}_1} ... \sigma^z_{\vec{R}_m} \sigma^z_{\vec{r}_1} ... \sigma^z_{\vec{r}_n} |\phi>, \tag{2.3}$$

with $\vec{k} \neq 0$. Here, $\{\vec{R}_i, \vec{r}_j\}_C$ means that the sum is over all $\{\vec{R}_1, ..., \vec{R}_m, \vec{r}_1, ..., \vec{r}_n\}$ with the constraint that no-two sites in the set are the same. These states are orthogonal; however, they do not form a complete set. The entire Hilbert space is spanned by

$$|...m_{\vec{k}}, m_{-\vec{k}}...> \equiv \prod_{\vec{k}, k_x>0} \left(\sqrt{\frac{[N-(m_{\vec{k}}+m_{-\vec{k}})]!}{m_{\vec{k}}! m_{-\vec{k}}! N!}} \sum_{\{\vec{R}_i, \vec{r}_j\}_C} e^{i\vec{k}.(\vec{R}_1+...+\vec{R}_{m_{\vec{k}}})} e^{-i\vec{k}.(\vec{r}_1+...+\vec{r}_{m_{-\vec{k}}})} \sigma^z_{\vec{R}_1} ... \sigma^z_{\vec{R}_{m_{\vec{k}}}} \sigma^z_{\vec{r}_1} ... \sigma^z_{\vec{r}_{m_{-\vec{k}}}} \right) |\phi>, \tag{2.4}$$

where $m_{\vec{k}}$ and $m_{-\vec{k}}$ are the number of magnons in the momentum states $\vec{k}$ and $-\vec{k}$ respectively. We can proceed further by introducing a separability approximation[28] in the calculation of the matrix elements of the unit operator and the Hamiltonian. Namely

$$< ...m'_{\vec{k}}, m'_{-\vec{k}}...|...m_{\vec{k}}, m_{-\vec{k}}... > \rightarrow \prod_{\vec{k},k_x>0} < m'_{\vec{k}}, m'_{-\vec{k}}|m_{\vec{k}}, m_{-\vec{k}} > = \prod_{\vec{k},k_x>0} \delta_{m'_{\vec{k}},m_{\vec{k}}} \delta_{m'_{-\vec{k}},m_{-\vec{k}}} \tag{2.5}$$

and

$$< ...m'_{\vec{k}}, m'_{-\vec{k}}...|H - E_\phi|...m_{\vec{k}}, m_{-\vec{k}}... > \rightarrow \sum_{\vec{q},q_x>0} < m'_{\vec{q}}, m'_{-\vec{q}}|H - E_\phi|m_{\vec{q}}, m_{-\vec{q}} > \times \prod_{\vec{k}\neq\vec{q},k_x>0} < m'_{\vec{k}}, m'_{-\vec{k}}|m_{\vec{k}}, m_{-\vec{k}} > . \tag{2.6}$$

where $E_\phi =< \phi|H|\phi >$. Since we have orthogonalized the states (2.3) for all $\vec{k}$, the states (2.4) are orthogonal within the separability approximation. This approximation makes sense only in a limited function space characterized by $1/N \sum_{\vec{k}} m_{\vec{k}} << 1$.

The eigenvalue problem can be solved exactly with the matrix elements of H calculated in the separability approximation. The ground-state energy is given by $E_0 = -\frac{Nd}{4} + d\sum_{\vec{k},k_x>0}\left(-1+\sqrt{1-\gamma(k)^2}\right)$. Evaluation of this expression for a large enough square lattice gives $\frac{E_0}{dN} = -0.3290$. This value is within $\sim 2\%$ agreement with the best estimates[12] of -0.3349 ± 0.0001. While the y and z component of the ground state sublattice magnetization vanishes, its x component is the same as in the SWT (for the square lattice we obtain 0.303 which is $\sim 61\%$ of its classical value). In the separability approximation the excitation spectrum is also the same as that obtained with linear SWT.

After some algebra[8], the ground-state wave-function in the separability approximation is obtained as

$$|\psi_0 >= \Lambda \exp\left(-\frac{1}{2}\sum_{i<j} u_{ij}\sigma_i^z\sigma_j^z\right)|\phi >, \tag{2.7.a}$$

where

$$u_{ij} \equiv \frac{1}{N}\sum_{\vec{k}}\left(\sqrt{\frac{1+\gamma(k)}{1-\gamma(k)}}-1\right)e^{i\vec{k}.(\vec{R}_i-\vec{R}_j)} \tag{2.7.b}$$

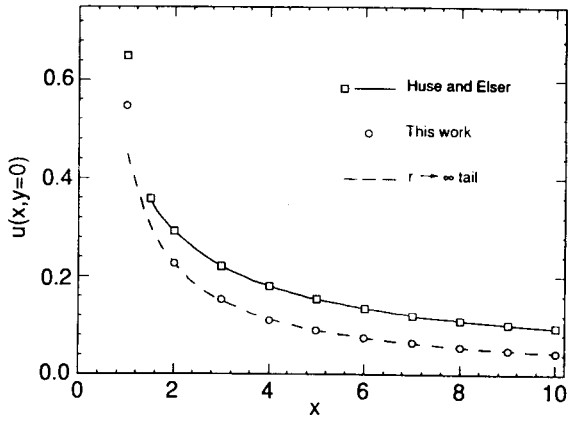

Figure 1. Our results for the exponent $u(x,y)$ of the correlation factors in the ground state wave-function (Eq. 2.7) (open circles) for $y = 0$. The solid line represents the results of the Variational Monte Carlo calculation of Huse and Elser.

where $\gamma(k) = 1/2(cosk_x + cosk_y)$. Variational wave-functions of similar form have been studied by Hulthen[29], Kastelijn[30], Marshall[31] and Bartkowski[32]. More recently the form (2.7.a) was studied by Huse and Elser [33] using the VMC approach. They took $u(1) = u_1$ and $u(r) = a/r^b$ for $r > 1$, where $r = |\vec{R}_i - \vec{R}_j|$ and treated u_1, a and b as variational parameters. The energy obtained in this approach[33] is $\sim -0.332J$ for $u_1 \sim 0.65$ $a \sim 0.475$ and $b \sim 0.7$. Similar VMC studies were carried out by Horsch and Linden[34] where using only $u(1)$ as a variational parameter (and $u(r > 1) = 0$) they found $-0.322J$ for the ground state energy in our units. Notice that our u is not a function of the distance r between two points on the lattice but rather a function of the two components x and y of the vector $\vec{R}_{ij}$. In Fig. 1 we plot our $u(x, y = 0)$ (open circles) and compare it with the results of Ref. 33. The form (2.7) has long-distance behavior consistent with the existence of long-wavelength spin-wave excitations. From Eq. (2.7.b) we find that

$$u(r \to \infty) = \frac{\sqrt{2}}{\pi r} \tag{2.8}$$

This form is shown by the dashed-line in Fig.1 and we note that the onset of the asymptotic form starts from essentially $r = 2$. In liquid ^4He the existence of long-wavelength excitations (zero sound) influences the long-range behavior of the Jastrow correlation factor[35]. The long-range behavior of the wave-function does not give

significant contribution to the ground-state energy. However, it has important consequences to the spectrum of elementary excitations when the same wave-function is used to define the Feynman-Cohen states or to construct a correlated basis[36]. We notice that the tails of the wave-function of Ref. 33 and that of Eq.(2.8) are quite different.

We have calculated the expectation value of the Heisenberg Hamiltonian with the wave-function (2.7.a-c) using MC integration. We have restricted the sum in (2.2) (which defines $|\phi>$ to be used in Eq. 2.7) to configurations with zero total z-component of S_z. We found almost the same energy (slightly better(lower)) with that of [33]. The advantage of the wave-function (2.7) is its simple physical origin and the fact that one obtains the same ground-state energy with no-free parameters. Next we improve the wave-function (2.7) further using sum-rules.

We can express the eigenstates of (1.5) as $|\Psi>=\sum_c \psi(c)(-1)^{L(c)}|c>$. The configuration $|c>$ can be labeled by the location of the down spins on the lattice i.e., $|c>=|i_1,i_2,...i_r>$ and the function $\psi(i_1,i_2,...,i_r)$ gives the amplitude of that configuration. The phase $(-1)^{L(c)}$ has been defined earlier and is separated from the amplitude ψ in order to obtain a non-negative ψ for any ground state configuration[31]. In this representation it is straightforward to show that the eigenvalue problem for the Hamiltonian (1.5) reduces to a difference equation for the amplitude $\psi(i_1,i_2,...,i_r)$ which is identical to the many-particle Schrödinger equation on a 2D lattice. In this quantum Boson lattice-gas the "particles" (the particles correspond to the down spins) have a "mass" $m=2$ in units $\hbar=J=1$ and interact via a pair potential V_{ij} having an infinite on-site repulsion, $V_{ij}=1$ if ij is a n.n pair and $V_{ij}=0$ otherwise. This is a useful representation because some of our knowledge about the system of Bose-particles can be translated to the magnetic system also. For example, Reatto and Chester have shown[35] that the zero-point motion of the long-wavelength modes of the Bose-system (zero-sound) gives rise to a long-range tail in the Jastrow wave-function. For a 2D system, we obtain

$$u(r\rightarrow\infty)=\frac{mc}{4\rho_0\pi r}, \tag{2.9}$$

where for the case of the quantum spin-1/2 system c is the spin-wave velocity, $m=2$ and $\rho_0=1/2$. The ground state of the spin-1/2 Heisenberg antiferromagnet has zero total S_z; therefore $\rho_0=1/2$, because the number of down spins is exactly half the total number of sites. Comparing the tails (2.8) and (2.9) we find the value for $c=\sqrt{2}$ found by linear SWT. Next, we discuss how to improve the wave-function (2.7) and calculate the spin-wave velocity using sum-rules.

We used three ω-moments (sum rules) of the dynamical structure function $S(\vec{q},\omega)$ to determine the spin-wave velocity, assuming that a single-magnon state exhausts them in the long-wavelength limit. Using the ω^0-moment (the static structure function $S(\vec{q})\equiv\langle 0|\sigma^z_{-q}\,\sigma^z_q|0\rangle$) and ω^1-moment we obtain

$$c=\frac{f}{s_1}, \tag{2.10}$$

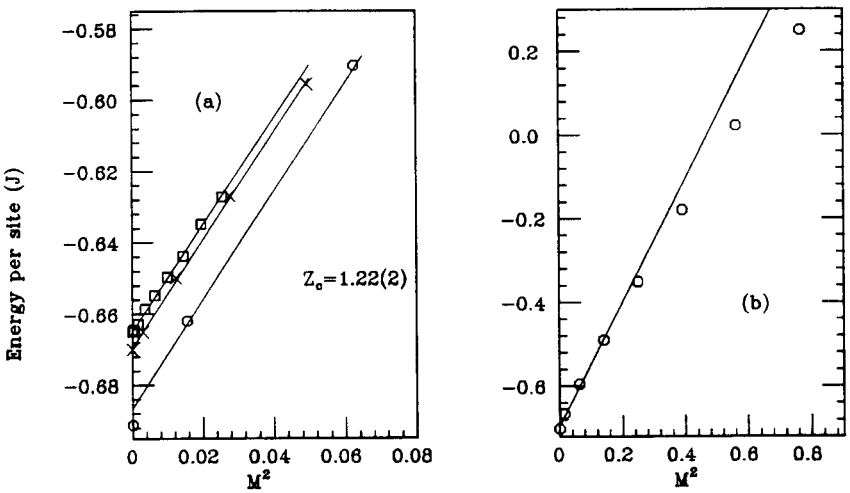

Figure 1. (a). The energy per site as a function of the square of the square of the total magnetization M^2 for 4×4, 6×6, and 10×10 lattices. The slope is related to the spin-wave velocity via Eq. 2.12. (b). Exact diagonalization results for ϵ versus M^2 obtained on a 4×4. The solid line has the same slope as the curves in fig (a).

where s_1 is the slope of $S(\vec{q})$ and

$$f \equiv -2J \sum_{\delta} \langle 0|(S_i^+ S_{i+\delta}^- + S_i^- S_{i+\delta}^+)|0\rangle. \tag{2.11}$$

The value of c calculated from Eq. 2.10 is sensitive to both the tail of the wave-function and finite size effects. As in the case of quantum liquids we use a different and more accurate way to determine c, explained next.

We have obtained[13] a third sum rule analogous to the compressibility sum rule in the case of quantum fluids which in the spin-system is translated to "magnetic susceptibility sum-rule" (ω^{-1} moment). Again assuming that this sum-rule is exhausted by a single-magnon-excitation we obtain

$$c = \sqrt{2f\epsilon''} \tag{2.12}$$

Here ϵ'' is the second derivative of the energy per particle $\epsilon(M)$ with respect to the magnetization density $M = 1/N < \sum_i \sigma_i^z >$. We note that the magnetization density corresponds to the particle density in the Bose system and the energy $\epsilon(M)$ to the ground-state equation of state. We calculate ϵ'' by restricting ourselves to a subspace

with well-defined S^z_{tot}, i.e., total z-component of the magnetization. Therefore we can determine the spin-wave velocity in a way analogous to that used in the case of quantum liquids to calculate the sound velocity. This technique is known to be accurate for numerical studies because it is not too sensitive to finite-size effects and to the tail of the ground-state wave-function.

In the variational calculation we used the form (2.7.a) including in the sum (2.2), defining $|\phi>$, configurations with zero total S_z only. We took $u(1)$ and $u(\sqrt{2})$ as variational parameters and

$$u(\vec{r}) = \alpha u_{LR}(\vec{r}), \quad for \quad \sqrt{x^2+y^2} \geq 2 \tag{2.13}$$

where $u_{LR}(\vec{r})$ is that given in Eq. (2.7.b) and α is a parameter of order 1. We did not treat α as a variational parameter because the ground-state energy is not too sensitive to its precise value. Instead it is determined self-consistently by satisfying the sum-rules.

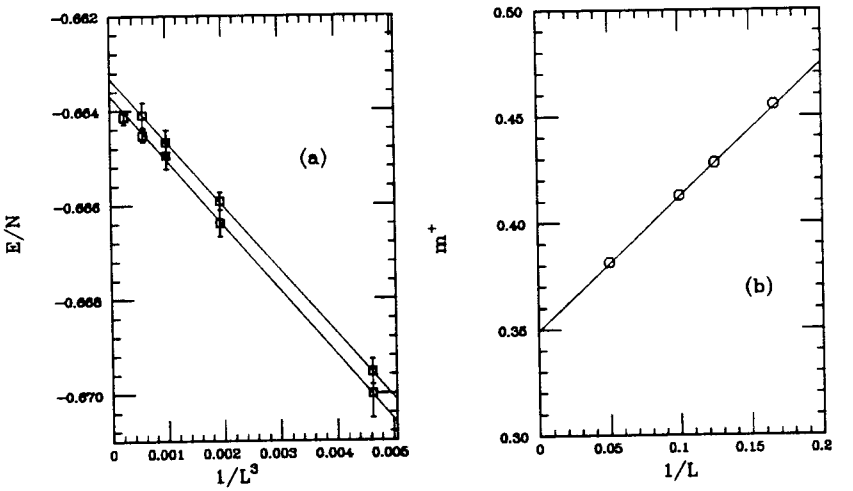

Figure 3. a) The energy per site as a function of L^{-3} for an L^2 lattice. The results are obtained with the parameter-free wave-function (2.7) (upper line) and with the improved wave-function (lower line). The energies are very close; The improved wavefunction is superior because it is consistent with sum-rules. b) The staggered magnetization versus L^{-1} with the improved wave-function.

Therefore, given a value of α we perform the variational calculation and determine $\epsilon(M)$ and the spin-wave velocity c from the slope of $\epsilon(M)$ via (2.12). Using the Reatto and Chester[35] relation (2.9) we obtain a new value for α from the relation $\alpha = c/\sqrt{2}$. This can be iterated until the input and the output value of α are the same. This procedure converges very quickly since as we mentioned the energy $\epsilon(M)$ is not sensitive to the value of α.

In Fig. 2.a we give $\epsilon(M)$ versus M^2 for several lattice sizes. Notice that ϵ'' is, within error bars, independent of the lattice size and we obtain $\alpha = 1.22 \pm 0.02$. The value of this parameter (commonly called Z_c) is in good agreement with the value 1.16 obtained by spin-wave theory[7] and the GFMC value[12] of 1.14 ± 0.05 recently reported. It is also the same with the slope obtained by exact diagonalization studies of a 4×4 lattice as shown in Fig. 2.b. Hence, we believe that the errors due to the approximate nature of our wave-function are small. Furthermore, we believe that in the GFMC calculation one may use our Eq. 2.12 to determine c more accurately. The calculated c using the form (2.10) has much larger errors as expected; it agrees, however, with the above value within error bars. In Fig. 3.a we present the ground state energy per site as function of L^{-3} for lattices of size $N = L^2$. The energy obtained with the wave-function (2.7.a-b) and with the improved wave-function (2.13) are the same within error bars. The extrapolated value for the infinite lattice is -0.6637 ± 0.0002. The advantage of the latter wave-function, however, is that it is consistent with sum rules and gives accurate excitation spectrum. Fig. 3.b shows the square root of the expectation value of the square of the staggered magnetization obtained with the improved wave-function as a function of L^{-1}. The extrapolation to the infinite-lattice gives $m^{\dagger} = 0.349 \pm 0.002$.

3. Heisenberg Antiferromagnet at Low Temperature and Nonlinear σ Model. Long Range Correlations.

Recently we simulated[16] the spin-1/2 2D AF Heisenberg model using Handscomb's quantum Monte Carlo method[37]. The calculated correlation length increases very rapidly with decreasing temperature and is consistent with that inferred from neutron scattering experiments. CHN studied the equivalent QNLσM by Renormalization Group with the β-function calculated with weak-coupling perturbation theory up to one[18] and two[19] loops. Their one-loop calculation suggests the form $\xi(T) = a/Te^{b/T}$ at low temperatures[18]. This form, however, does not fit the $\xi(T)$ obtained from the QMC calculation of the Heisenberg model[16]. Later, the two-loop calculation[19] of CHN gives a different prefactor namely, $\xi(T) = ae^{b/T}$. Using both MC simulation and saddle point approximation we have studied[20] this model to determine the correct behavior of $\xi(T)$ and to make contact between the two models. We found that in the ordered phase of the QNLσM, $\xi(T)$ can be approximated by

the second form which also agrees with $\xi(T)$ obtained from the QMC study of the Heisenberg model. Our $\xi(T)$ agrees reasonably well with the neutron scattering data using $J = 1270K$. Next, we review our main results and make contact between the two models.

The nonlinear σ model in two-space one-Euclidean time dimensions is defined as[17]

$$S_{\text{eff}} = \frac{\rho_0}{2\hbar c}\int_0^{\beta\hbar c} d\tau \int dxdy\Big((\partial_x\vec{\Omega})^2 + (\partial_y\vec{\Omega})^2 + (\partial_\tau\vec{\Omega})^2\Big). \tag{3.1}$$

Here $\vec{\Omega}$ is a three-component vector field living on a unit sphere, c is the spin-wave velocity and $\beta = \frac{1}{K_B T}$. We discretize the space-time and put the model on the 2+1 dimensional lattice:

$$S_{\text{eff}} = -\frac{1}{2g}\sum_{\vec{x}}\sum_{\mu=1}^{3}\vec{\Omega}(\vec{x}).\Big(\vec{\Omega}(\vec{x}+\hat{e}_\mu) + \vec{\Omega}(\vec{x}-\hat{e}_\mu)\Big), \tag{3.2}$$

where $g = \hbar c/\rho_0 a$ and $\vec{x}$ covers the 2+1 dimensional lattice of lattice spacing a, size $N^2 N_\beta$ and

$$\beta\hbar c = N_\beta a. \tag{3.3}$$

In this model the average of the field $\vec{\Omega}$ is proportional to the average staggered magnetization and could describe the spin-dynamics within one isolated CuO_2 layer.

From the two-point function we calculated the correlation length ξ_{latt} in lattice units as a function of g, N_β and N. It is known that for $g > g_c$, where g_c is the 3D critical point ($T = 0$), the three modes of the theory have degenerate finite masses (inverse correlation lengths). For $g < g_c$, however, there are two masses in the theory. There are two modes which become massless (Goldstone-modes) in the 3D theory ($\beta \to \infty$) and they are related to the radial motion of the average field. There is also a massive mode associated with fluctuations in the magnitude (radial component) of the average field. Next, we discuss the mode having the smallest mass, which dominates the behavior of the correlation function at large distances. For continuum limit behavior and for eliminating finite-size effects ξ_{latt} must satisfy $1 << \xi_{\text{latt}} << N$. If, therefore, N is large enough so that $\xi_{\text{latt}} << N$, the correlation length is only a function of N_β and g. In physical units ξ is given by

$$\xi = \xi_{\text{latt}}(g, N_\beta)a. \tag{3.4}$$

To keep the correlation length ξ constant in physical units, for any $a \to 0$ we should find the value of g which gives the same value of ξ. This is achieved through Eq. (3.4) which defines the function $g(a)$. The combination of Eq. (3.3) and Eq. (3.4) gives: $\xi = b\frac{\hbar c}{K_B T}$, where $b = \frac{\xi_{\text{latt}}(g,N_\beta)}{N_\beta}$. In order to keep ξ constant at a fixed temperature we should keep the ratio b constant. b is the physical value of the correlation length at temperature T in units of $a_T \equiv \frac{\hbar c}{K_B T}$. In Fig.4 we give b as a function of g for several values of N_β. We notice that the lines for various N_β pass

through the same point $(g_c, b^*) = (1.45 \pm 0.01, 0.80 \pm 0.05)$. Let us say, that we would like to define the theory's coupling constant at the value $b = b_0$ shown in Fig.4. The line $b = b_0$ intersects the various curves for different N_β's (i.e., in this case in which the temperature is constant for different a's), and the value of g at the intersections define $g(a_T/N_\beta)$. We note that $\lim_{N_\beta \to \infty} g(a_T/N_\beta) = g_c$. At $g = g_c$ we obtain

$$\xi^* = b^* \frac{\hbar c}{K_\beta T}, \tag{3.5}$$

where $b^* = 0.80 \pm 0.05$. Notice that at $T = 0$, g_c turns into a critical point.

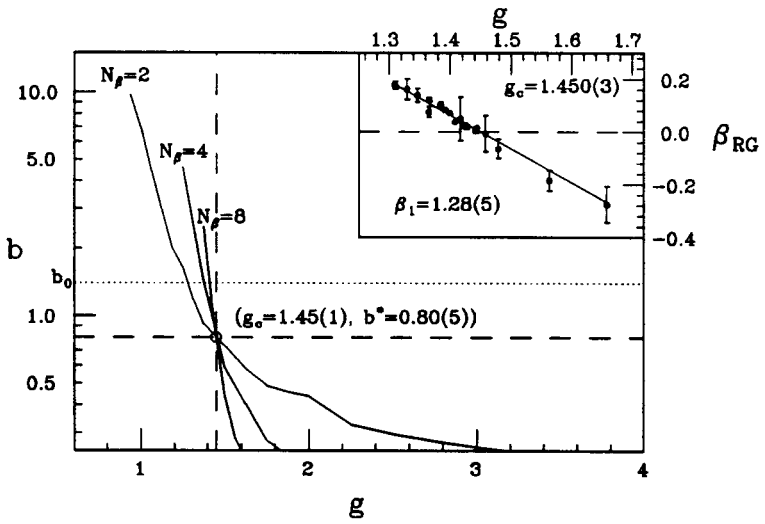

Figure 4. The ratio $b = \xi_{\rm latt}/N_\beta$ versus g for different N_β. Notice that all the lines for different N_β pass trough the same point (g_c, b^*). The inset shows the renormalization group β-function.

Using correlation lengths obtained on lattices of sizes $50^2 \times N_\beta$ and $100^2 \times N_\beta$ with $N_\beta = 2, 4, 6, 8$, we calculate the renormalization group β-function $\beta_{RG} \equiv -a\frac{dg(a)}{da}$. Our results for β_{RG} are shown in the inset of Fig.4. At $g = g_c$, β_{RG} changes sign. At $T = 0$, $\xi^* = \infty$, and for $g < g_c$ the system enters in a phase with spontaneous symmetry breaking, where the staggered magnetization is non-zero. We see that close to the critical point $\beta_{RG}(g)$ is linear:

$$\beta_{RG}(g) = -\beta_1(g - g_c) + \ldots. \tag{3.6}$$

We find $g_c = 1.450 \pm 0.003$ and $\beta_1 = 1.28 \pm 0.05$. Integrating both sides of the equation defining β_{RG} one obtains $a(g) = a_\sigma e^{-\int^g \frac{dg}{\beta_{RG}(g)}}$ where a_σ is a constant of integration having dimensions of length. Using the linear approximation for β_{RG} close to the critical point we find

$$a(g) = a_\sigma |g - g_c|^{\frac{1}{\beta_1}}. \tag{3.7}$$

Combining Eq.(3.3-4) and Eq.(3.7) we obtain

$$\frac{T}{T_\sigma} = \frac{1}{N_\beta |g - g_c|^{\frac{1}{\beta_1}}}, \tag{3.8}$$

$$\frac{\xi}{a_\sigma} = \xi_{latt}(g, N_\beta)) |g - g_c|^{\frac{1}{\beta_1}}. \tag{3.9}$$

where $K_B T_\sigma = \frac{\hbar c}{a_\sigma}$. The constants a_σ and T_σ are independent of g and a. The function $\xi_{latt}(g, N_\beta)$ is known for several values of g and N_β from our MC calculation. Given a value for g and N_β, using (3.8) and (3.9), we can find the temperature $t = T/T_\sigma$ (in units of T_σ and the corresponding value of the correlation length ξ/a_σ in units of a_σ. In Fig.5 we show the function ξ/a_σ versus $t = T/T_\sigma$ found in this way. We see that all points scale to a universal curve $f(t)$. We notice the occurrence of dimensional transmutation where, although the lattice spacing is removed together with g, we obtain correlation lengths in units of a finite length scale a_σ as a function of temperature t in units of T_σ. The curve $f(t)$ can be approximated by an exponential:

$$f(t) = A_\sigma \exp(B_\sigma / t), \tag{3.10}$$

as the saddle point approximation[20] and the most recent work of CHN[19] suggest. The best fit gives $A_\sigma = 0.0795$ and $B_\sigma = 4.308$ and it is shown as a solid line in Fig.5.

For $g >> g_c$ the correlation length in the nonlinear σ model is only a function of g and is independent of T. At the critical point $g = g_c$ we find that at low T, ξ grows as $1/T$ as the temperature decreases. We have compared our numerical results with results obtained in the saddle point approximation. We find good agreement in the region $g > g_c$, but poor agreement for $g < g_c$.

It is possible to make contact between the S=1/2 antiferromagnetic Heisenberg model and nonlinear σ model. In Ref.16, we fit the correlation lengths to two different forms

$$\xi(T) = C/T e^{b/T}, \tag{3.11}$$

and

$$\xi(T) = C e^{b/|T - T_c|^{1/2}}. \tag{3.12}$$

and we found that the latter form fits better and concluded that our simulation indicated that either we need to reach lower temperatures for the form (3.11) to be valid or that topological excitations may play an important role in the dynamics of the Spin-1/2 Heisenberg antiferromagnet. Following our findings for the σ model and

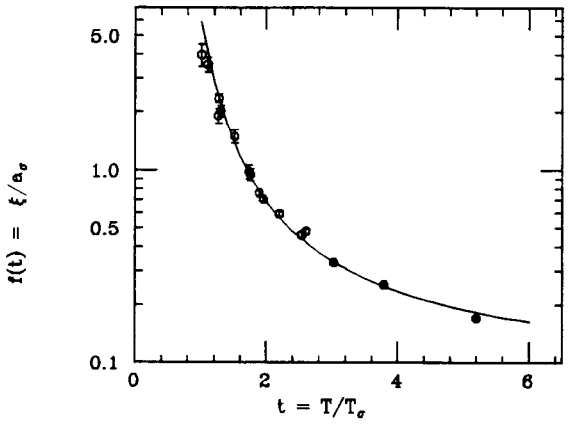

Figure 5. The function $f(t)$(see text for definition). Our data for various g's collapse on the same curve by using the calculated renormalization group β-function. The solid line corresponds to an exponential fit.

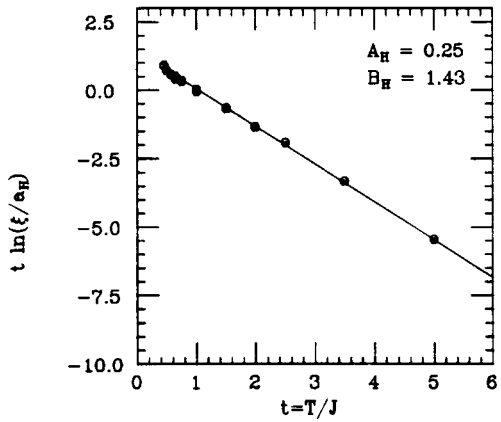

Figure 6. Demonstration that the correlation length as a function of T can be approximated by $ae^{b/T}$.

the revised suggestion of CHN[19] we attempt to fit our numerical results for the Heisenberg model to

$$\xi/a_H = A_H \exp(B_H J/T). \tag{3.13}$$

This form, i.e., without the $1/T$ prefactor, fits very well our data as demonstrated in Fig. 6, giving $A_H = 0.25$ and $B_H = 1.4$. Similar values have been reported in Ref. 38. On this basis we may conclude that the results of our simulation are consistent with SWT and existence of an ordered state at $T = 0$.

Let us assume that the two models are equivalent at low T. In order to obtain the best fit between the calculated correlation length for the two models, we need to assume that the spin-1/2 AF Heisenberg model corresponds to the broken phase($g < g_c$) of the σ model in the continuum limit. Therefore the spin-1/2 AF Heisenberg model should order at $T = 0$ and $A_H a_H = A_\sigma a_\sigma$ and $B_H J = B_\sigma T_\sigma$. We obtain $T_\sigma = 0.325J$ and $a_\sigma = 3.14 a_H$.

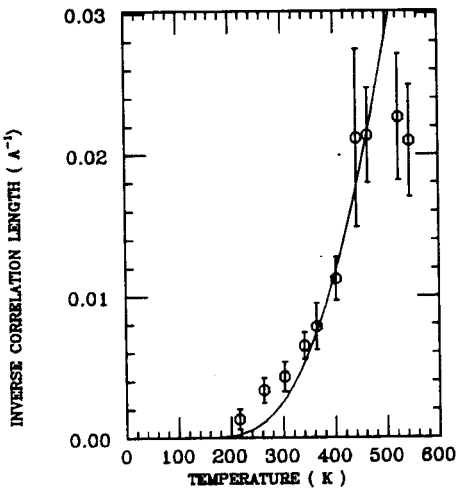

Figure 7. The solid line corresponds to an exponential fit to both our results for the nonlinear σ model and the spin-1/2 AF Heisenberg model. We used the value $J = 1270K$ for the AF coupling. The open circles with error bars are neutron scattering data taken on the insulator La_2CuO_4.

In Fig.7 we plot the inverse correlation length versus T as observed by neutron scattering experiments[14]. The solid curve is the exponential given by Eq. 3.13 which fits the results for $\xi(T)$ obtained from the nonlinear σ model and AF Heisenberg model. In the plot we used $a_H = 3.8\mathring{A}$, the $Cu - Cu$ distance, and $J = 1270K$ which is close to the value reported by Raman scattering experiments[39]. Using this value of J and the expression $c = 1.22\sqrt{2}Ja$ we obtain $c = 0.72eV - \mathring{A}$, a value higher than the lower bound of $0.6eV\mathring{A}$ reported by thermal neutron scattering studies[14] and lower than the more recent value of $0.85eV\mathring{A}$ inferred form high-energy inelastic

neutron scattering[15]. It is interesting, however, that we can achieve this agreement with no-free parameters. Our curve disagrees with the data very close to the 3D Nèel critical temperature $T_N \sim 200K$. Smaller values of J will bring our results closer to the data in that region but further away from the data at higher T.

4. Holes in a Quantum Antiferromagnet.

Several authors[3,21,22,23,24] have studied the motion of a single hole as described by the Hamiltonian (1.1-4) or the $t-J$ model using perturbation or variational theory and exact diagonalization of finite clusters. It has been found that the hole, moving in an antiferromagnetic background distorted in the neighborhood of the hole, is transformed into a well-defined quasiparticle. This quasiparticle excitation is separated by a small gap from an incoherent spectrum of spin-excitations. The minimum of the hole-band is located at $\vec{k} = (\frac{\pi}{2}, \frac{\pi}{2})$, the bandwidth is of order J/t for large J/t and the hole-quasiparticle strength relative to the total strength of the spectral function increases with J/t.

The paired-magnon analysis can guide us to construct a wave-function for the single-hole. Following the mapping of the Heisenberg model to the Boson lattice-gas model a hole in a quantum antiferromagnet can be mapped to an impurity moving in a Bose system. A variational wave-function which includes spin-spin and spin-hole correlations is the following

$$|\Psi(\vec{k})>= \frac{1}{\sqrt{N}}\sum_{\vec{R}} e^{-i\vec{k}\cdot\vec{R}}\hat{G}_{\vec{k}}|\phi(\vec{R})> \tag{4.1}$$

with $|\phi(\vec{R})>$ is the state (2.2) with the hole at $\vec{R}$. The correlation operator $\hat{G}_{\vec{k}}$ has the following form

$$\hat{G}_{\vec{k}} = exp\Big(-\frac{1}{2}\sum_{\vec{r}} h(\vec{r})e^{-i\vec{k}\cdot\vec{r}}s^z_{\vec{R}+\vec{r}} - \frac{1}{2}\sum_{ij} u(ij)s^z_i s^z_j\Big). \tag{4.2}$$

This wave function can be obtained from perturbation theory of the $t-J$ model in the limit $t/J_z, J\perp/J_z << 1$. It contains the main pair (spin-spin and spin-hole) correlations. The origin of the second term is the same as that in the pure Heisenberg model and creates spin fluctuations (the $|\phi>$ state is a Nèel state in the x-direction therefore the $s^z_i s^z_j$ term creates pair-fluctuations). The first term couples the almost Nèel state with the state where the hole hops to a neighboring site. It may be interesting to notice that this wave-function is the translation for the case of the

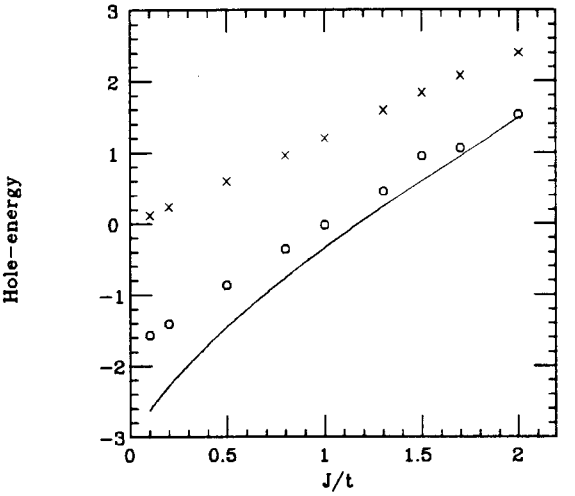

Figure 8. Hole energy for $\vec{k} = (\frac{\pi}{2}, \frac{\pi}{2})$ as a function of J/t. The solid line are exact diagonalization results[24], while the crosses and circles are obtained with the variational wavefunction function (4.1-2) with $h = 0$ and $h \neq 0$ respectively.

spin-system of the Feynman-Cohen[40] wave-function for the elementary excitations in liquid ^4He which takes into account the backflow correlations.

In general u_{ij} may depend on the distance from the hole. In practice we find no significant lowering of the hole energy by allowing for such a non-uniform u_{ij}. We, therefore, used the same u_{ij} as that found in the VMC calculation at half-filling (Heisenberg model) which is explained in section 2. The hole energy is sensitive to $h(1)$ but not very sensitive to $h(\tau > 1)$. Using the Metropolis algorithm we calculated[27] the expectation value of the tJ Hamiltonian (the $t - J$ model is obtained from (1.1) simply by neglecting H_3 and substituting $U = 4t^2/J$ in the H_2 term) with the wave-function (4.1-2) for one hole.

Fig.8 compares our variational results for the energy of a hole (we have substracted the energy of the no-hole state) moving with $\vec{k} = (\frac{\pi}{2}, \frac{\pi}{2})$ for the two cases, $h = 0$ and for the optimal value of h, with exact diagonalization results on the 4×4 lattice [24] for several values of J/t. The introduction of the spin-hole correlations ($h \neq 0$) improves the energy significantly. The variational wave-function performs best when $J/t \geq 1$; for lower values of J/t we need to improve the wave-function to include two- or higher-hop processes. Similar results are found for the 10×10 lattice. The single-hole energy $e(\vec{k})$ (we have not substracted the no-hole energy in this case) as a function of the momentum $\vec{k}$ is calculated for several values of J/t. A typical

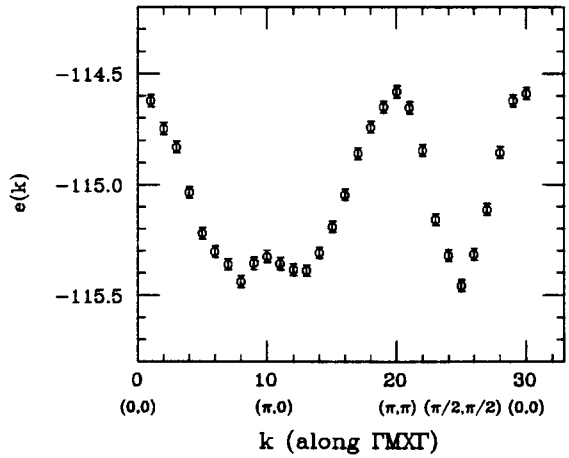

Figure 9. The hole-band $e(\vec{k})$.

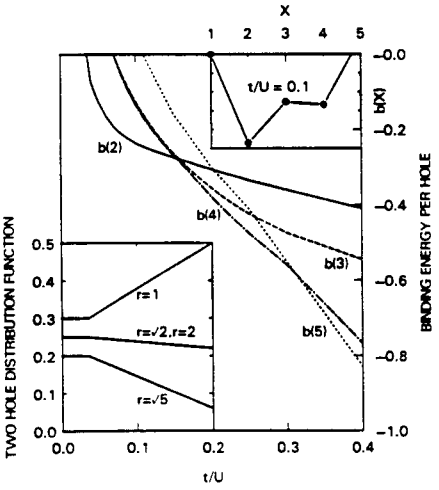

Figure 10. The binding energies per hole $b(X)$ for a system of X holes as a function of t/U. The lower-left inset gives the hole-hole distribution function for various distances. The top-right inset demonstrates the "magic" numbers for even number of holes. See text for more details.

result is shown in Fig. 9 calculated for $J/t = 1$ on a 10×10 lattice. The curve features a minimum at $\vec{k} = (\frac{\pi}{2}, \frac{\pi}{2})$. The maximum value is at $\vec{k} = (0,0)$ or $\vec{k} = (\pi, \pi)$ and both values are the same within error bars. The bandwidth decreases with J/t. We also find, in agreement with other authors[22,23], that the effective mass of the hole in the direction towards $(0, \pi)$ is larger than that in the direction towards $(0,0)$.

Next, we briefly discuss our main results obtained by exact diagonalization of the full Hamiltonian (1.1) on finite clusters of 10-sites[3]. In this work we have included the H_3 term. In Fig. 10 we plot the binding energy per hole defined as

$$b(X) = \frac{E(X) - XE(1)}{X} \tag{4.3}$$

where $E(X)$ is the total energy of the system containing X holes, measured from the energy of the no-hole state (i.e., we have taken E(0)=0). Notice that there is a range of t/U where two-hole pairing is favored against multi-hole pairing or phase separation. The lower left inset shows the hole-hole distribution function and the top-right inset shows $B(X)$ versus X. The latter inset demonstrates that the peaks in $b(X)$ occur at even hole numbers. This calculation has been recently reproduced in Ref. 25. In addition, in Ref. 25, it was found that the pairing is predominantly d-wave.

5. Acknowledgements

This work was supported in part by U.S. Defense Advanced Research Projects Agency (DARPA) sponsored Florida Initiative in Advanced Microelectronics and Materials under Contract No. MDA972-88-J-1006.

6. References

1. P. W. Anderson, *Science* **235**, 1196 (1987).
2. J.E. Hirsch, Phys. Rev. Lett. **54**, 1317 (1985). K. Huang and E. Manousakis, Phys. Rev. **B36**, 8302 (1987).
3. E. Kaxiras and E. Manousakis, Phys. Rev. **B38**, 866 (1988) and Phys. Rev. **B37**, 656 (1988).
4. B. Friedman, X. Y. Chen, and W. P. Su, Phys. Rev. **B40**, 1 September issue. E. Kaxiras and E. Manousakis, Phys. Rev. **B40**, 2596 (1989).
5. N. D. Mermin and H. Wagner, Phys. Rev. Lett. **22**, 1133 (1966).
6. K. Kubo Phys. Rev. Lett. **61**, 110 (1988). K. Kubo and T. Kishi, Phys. Rev. Lett. **61**, 2585 (1988).
7. P. W. Anderson, Phys. Rev. **86**, 694 (1952). R. Kubo, Phys. Rev. **87**, 568 (1952). T. Oguchi, Phys. Rev. **117**, 117 (1960).
8. E. Manousakis, Phys. Rev. **B40** (1989) 1 September issue.
9. M. Parrinello and T. Arai, Phys. Rev. **B10**, 265 (1974). D. Huse, Phys. Rev. *B37*, 2380 (1988).
10. J. Oitmaa and D.D. Betts, Can. J. Phys. **56**, 897 (1978).

11. J. D. Reger and A. P. Young, Phys. Rev **B37**, 5978 (1988). S. Miyashita, J. Phys. Soc. Jpn. **57**, 1934 (1988). T. Barnes, Phys. Rev. **B37**, 9405 (1988). Y. Okabe and M. Kicuchi, J. Phys. Soc. Jpn. **57**, 4351 (1988). M. Gross, E. Sànchez-Velasco and E. Siggia, Phys. Rev. **B39**, 2484.
12. J. Carlson, Phys. Rev. **B40**, 846 (1989). N. Trivedi and D. Ceperley, *ibid.* **B40**, 2747 (1989).
13. Z. Liu and E. Manousakis, to be published.
14. D. Vaknin, S.K.Sinha, D.E. Moncton, D.C. Johnston, J.M. Newsam, C.R. Safinya and H.E. King, Jr. Phys. Rev. Lett. **58**, 2802 (1987). G. Shirane, Y. Endoh, R.J.Birgeneau, M. A. Kastner, Y. Hidaka, M. Oda, M. Suzuki, and T. Murakami, Phys. Rev. Lett. **59**, 1613 (1987). Y. Endoh, et al., Phys. Rev., **B37**, 7443 (1988).
15. G. Aeppli, et al., Phys. Rev. Lett. **62**, 2052 (1989).
16. E. Manousakis and R. Salvador, Phys. Rev. Lett. **60**, 840 (1988). E. Manousakis and R. Salvador, Phys. Rev. **B39**, 575 (1989).
17. F. D. M. Haldane, Phys. Lett. **93 A**, 464 (1983); Phys. Rev. Lett. bf 50, 1153 (1983). T. Dombre and N. Read, Phys. Rev. **B 38**, 7181 (1988); E. Fradkin and M. Stone, *ibid* **38**, 7215 (1988); L. B. Ioffe and A. I. Larkin, Int. J. Mod. Phys. **B 2**, 203 (1988); X.-G. Wen and A. Zee, Phys. Rev. Lett. **61**, 1025 (1988), F.D.M. Haldane, *ibid* **61**, 1029 (1988).
18. S. Chakravarty, B.I. Halperin, and D. Nelson, Phys. Rev. Lett. **60**, 1057 (1988).
19. S. Chakravarty, B.I. Halperin, and D. Nelson, Phys. Rev. **B39**, 2344 (1989).
20. E. Manousakis and R. Salvador, Phys. Rev. Lett. **62**, 1310 (1989); and Phys. Rev. **B40**, 2205 (1989).
21. B.Shraiman and E.Siggia, Phys. Rev. Lett. **60**, 740 (1988).
22. C.L.Kane, P.A. Lee, and N.Read, Phys. Rev. **B39**, 6880 (1989). S. Schmitt-Rink, C. M. Varma, and A. E. Ruckenstein, Phys. Rev. Lett. **60**, 2793 (1988).
23. C.Gros and M.D.Johnson, to be published.
24. E.Dagotto, A.Moreo, R.Joynt, S.Bacci, and E. Gagliano, NSF-ITP-89-74, May, 1989.
25. J. A. Riera and A. P. Young, Phys. Rev. **B 39**, 9697 (1989).
26. J.E. Hirsch and S. Tang, Phys. Rev. Lett. **62** ,591 (1989).
27. M. Boninsegni and E. Manousakis, to be published.
28. E. Feenberg, *Theory of Quantum Fluids*, Academic Press, New York and London (1969).
29. L. Hulthen, Ark. Mat. Astr. Fys., **26A**, No. 1 (1938).
30. P. W. Kastelijn, Physica **18**, 104 (1952).
31. W. Marshall, Proc. R. Soc. London, Ser. A **232**, 48 (1955).
32. R. Bortkowski, Phys. Rev. **B5**, 4536 (1972).
33. D. A. Huse and V. Elser, Phys. Rev. Lett. **60**, 2531 (1988).
34. P. Horsch and W. von der Linden: Z. Phys. **B72**, 181 (1988).
35. G. V. Chester and L. Reatto, Phys. Lett. **22**, 276 (1966).
36. E. Manousakis and V. R. Pandharipande, Phys. Rev. B **30**, 5062 (1984).
37. D. C. Handscomb, Proc. Camb. Phil. Soc. **58**, 594 (1962) and **60**, 115(1964). J. W. Lyklema, Phys. Rev. Lett. **49**, 88 (1982). D.H. Lee, J.D. Joannopoulos and J.W. Negele, Phys. Rev. **B30**, 1599 (1984).
38. G. Gomez-Santos, J. D. Joannopoulos and J. W. Negele, Phys. Rev. **B39**, 4435 (1989).
39. K. B. Lyons, P.A. Fleury, J.P.Remeika and T.J. Nergan, Phys. Rev. **B37**, 2353 (1988).
40. R. P. Feynman and M. Cohen, Phys. Rev. **102**, 1189 (1957).